Energy Reports 12 (2024) 775–786

Contents lists available at ScienceDirect

Energy Reports

journal homepage: www.elsevier.com/locate/egyr

Enhancing hydrogen generation through advanced power conditioning in renewable energy integration

Omar Abdel-Rahim [a,b,*], Thamer A.H. Alghamdi [c,d], Wesam Rohouma [e,*], Adel B. Abdel-Rahman [b]

[a] Department of Electrical Engineering, Aswan University, Aswan 81542, Egypt
[b] Department of Electrical Engineering, Egypt-japan University of Science and Technology, Alexandria, Egypt
[c] Wolfson Centre for Magnetics, School of Engineering, Cardiff University, Cardiff CF24 3AA, UK
[d] Electrical Engineering Department, School of Engineering, Al-Baha University Al-Baha 65779, Saudi Arabia
[e] Electrical power and renewable energy, University of Doha for Science and Technology, Qatar

ARTICLE INFO

Keywords:
Hydrogen
DC-DC
AC-DC
12-pulse diode rectifier
Matrix converter

ABSTRACT

Producing hydrogen using renewable energy is a pivotal move towards cleaner and eco-friendlier energy generation, playing a vital role in safeguarding the environment. This method merges power electronic tools with electrolysers, which are key in enhancing hydrogen creation efficiency. Given that electrolysis operate on direct current (DC) voltage, there's a need for DC-DC or AC-DC converters to guarantee the right voltage and current for optimal electrolysis. This study aims to present a power regulation system tailored for hydrogen production powered by renewable resources. This system consists of two main stages: the matrix converter and the 12-pulse diode rectifier. The matrix converter ensures a controlled intake of current from the alternating current (AC) side, leading to a sinusoidal output with limited harmonic disruption. Additionally, it produces an AC voltage with a controlled magnitude and frequency, designed to suit the 12-pulse diode rectifier that follows. This meticulous voltage control is fundamental, granting enhanced operational adaptability and producing a high-quality waveform to support the electrolysis. Finally, the 12-pulse diode rectifier's task is to transform the AC from the matrix converter into a consistent DC voltage, crucial for effective hydrogen production.

1. Introduction

Hydrogen stands out as a multifaceted energy medium that can be derived from various resources and leveraged in multiple applications. Among its potential uses, hydrogen's role in power generation promises not only enhanced energy efficiency but also environmental benefits and potential economic gains (Carmo et al., 2013; Moradi and Groth, 2019; Buttler and Spliethoff, 2018). When used in fuel cells or internal combustion engines, hydrogen combustion results in just water as a residue. Adopting hydrogen for power generation can curtail carbon emissions from conventional power sources and augment the incorporation of renewables (Staffell and Green, 2019; Brouwer, 2010). Concentration overvoltage is typically negligible when operating below a current density of 1 A/cm^2. Some experts believe that concentration over potential becomes significant only at extremely high current densities, suggesting it wouldn't be a major concern for the proton exchange membrane (PEM) electrolysers found in most commercial applications (Brouwer, 2010). Electrolysis, a prevalent method for hydrogen generation, employs electric current to disintegrate water into hydrogen and oxygen. Powering electrolysis with renewables like solar and wind renders it an environmentally friendly and sustainable hydrogen production method. Nonetheless, electrolysis efficiency can be hampered by the power electronics governing the electric current. As a DC load, the water electrolyser needs either AC/DC or DC/DC power conditioning. By adeptly managing the power conditioning phase, the desired output power can be set. The electrolyser's power output is gauged by the I-V curve, which is sensitive to both temperature and pressure during operation. The electrolyser cell stack's current, denoted by its mean value, signifies the amount of hydrogen generated over a specific period. Fig. 1 underlines that concentration overvoltage is considerably pronounced in PEM electrolysis, yet in alkaline electrolysis, where current densities are typically under 0.5 A/cm^2, it's less influential (Mazloomi and Sulaiman, 2012; De Lorenzo et al., 2022).

* Corresponding author at: Department of Electrical Engineering, Aswan University, Aswan 81542, Egypt.
* Corresponding author.
E-mail addresses: o.abdelrahim@aswu.edu.eg (O. Abdel-Rahim), wesam.rohouma@udst.edu.qa (W. Rohouma).

https://doi.org/10.1016/j.egyr.2024.06.049
Received 28 November 2023; Received in revised form 2 June 2024; Accepted 19 June 2024
Available online 4 July 2024

Nomenclature

(PEM)	proton exchange membrane
(PV)	photovoltaic
(FC)	fuel cell
(UC)	ultra-capacitor
(PEPT)	power electronic phase-shifting transformer
(IPR)	inter-phase reactor
(THD)	total harmonic distortion
(OC)	open-circuit
(ATRU)	autotransformer rectifier unit
(MC)	Matrix Converter
(MPC)	Model Predictive Control
(MIMO)	multi-input multi-output

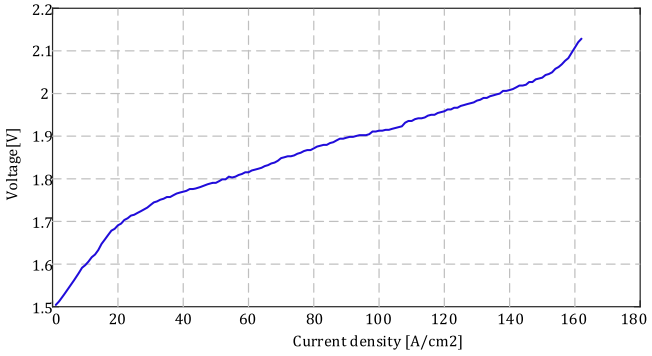

Fig. 1. Relation between voltage level and current concentration in Hydrogen Elecctrolyser.

The role of power electronics is vital in ensuring efficient and dependable hydrogen extraction. This process entails extracting hydrogen from water or other mediums using electrolysis or other techniques such as thermochemical, photochemical, or biological processes. Power electronics can offer the required voltage and current management, power quality enhancement, and energy governance for varied hydrogen extraction systems ↱ (Uzunoglu et al., 2009a; Meng et al., 2018a, 2019).

Uzunoglu, et al (Uzunoglu et al., 2009a). focuses on integrating photovoltaic (PV), fuel cell (FC), and ultra-capacitor (UC) systems to create a hybrid power generation system for sustained power supply in stand-alone applications ↱ (Uzunoglu et al., 2009a). The paper also presents mathematical and electrical models for the PV system, including a modified model for silicon solar PV panels to integrate the electrolyzer and FC-UC system. The paper does not discuss the scalability or applicability of the proposed system for larger or different types of stand-alone applications. Meng, et al (Meng et al., 2018a). proposed a 12-pulse rectifier based on a power electronic phase-shifting transformer (PEPT) to reduce the volume of the rectifier and improve power density. The proposed topology converts power frequency AC voltage into high-frequency voltage, which is then phase-shifted by a high-frequency transformer and sent to two sets of three-phase rectifier bridges for rectification. Simulations and experiments confirm the effectiveness and feasibility of the proposed topology. Meng et al. (2019). proposed a novel multi-pulse rectifier that combines a dual-passive-harmonic-reduction method and a traditional double-star uncontrolled rectifier. The method includes a multi-winding inter--phase reactor (IPR) and an auxiliary circuit. The turn ratio of the multi-winding IPR is optimally designed to minimize the total harmonic distortion (THD) of the input line current. Under the optimal turn ratio, the proposed rectifier operates as an 18-pulse rectifier, with a theoretical THD of about 10.1 % and an experimental THD of 6.58 %. Abdollahi et al. (2021). proposed 36-PR uses a PTC and a ZSBT circuit to ensure independent operation of the autotransformer output voltages and suppress circulating current. It has less rating, weight, volume, and cost compared to other conventional 36-PRs. The PTC is used to reduce kVA rating and input current THD, making it suitable for retrofit applications. The proposed structure achieves nearly sinusoidal waveforms for input line voltage and currents, with low THD values well below the defined standards. The performance of the proposed 36-PR is compared with other multi-pulse rectifiers (MPR) in terms of cost, power factor, and load rating.

Du et al. (2022a) The paper proposes a 12-pulse rectifier based on a power electronic phase-shifting transformer (PEPT) to reduce the volume of the rectifier and improve power density. The proposed topology converts power frequency AC voltage into high-frequency voltage, which is then phase-shifted by a high-frequency transformer and sent to two sets of three-phase rectifier bridges for rectification. Simulations and experiments confirm the effectiveness and feasibility of the proposed topology. Yang, et al (Uzunoglu et al., 2009b). investigated two types of open-circuit (OC) faults in a delta-polygon 18-pulse autotransformer rectifier unit (ATRU) used in aviation aircraft. It quantitatively analyzes the effects of diode OC faults on various aspects such as diode conduction angle, output voltage ripple, winding current, input current harmonics, and diode and transformer winding losses. It also examines the operating characteristics of the ATRU under input OC faults and discusses a fault diagnosis idea based on the affected intervals of the DC output voltage. The paper concludes by validating the theoretical analysis and discussion through simulation and experimental results, emphasizing the significance of this work for guiding fault detection, fault location, and predictive maintenance of ATRUs. Meng, et al (Du et al., 2022b). The paper proposes a novel multi-pulse rectifier that combines a dual-passive-harmonic-reduction method with a traditional double-star uncontrolled rectifier. The method includes a multi-winding inter-phase reactor (IPR) and an auxiliary circuit. The turn ratio of the multi-winding IPR is optimally designed to minimize the total harmonic

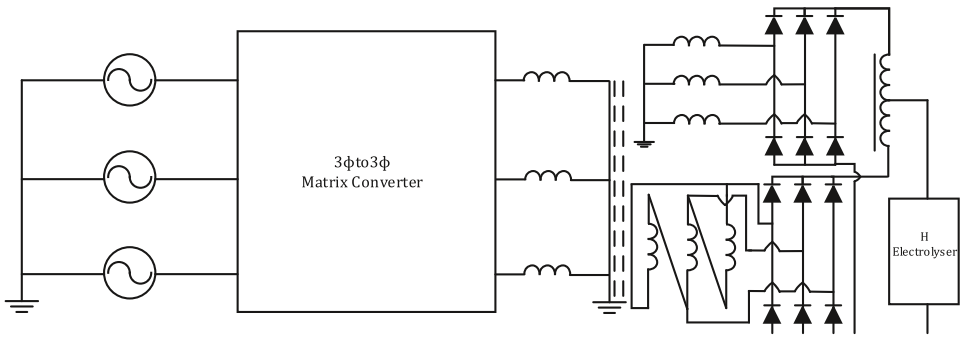

Fig. 2. General schematic of the proposed Hydrogen generation power conversion system.

distortion (THD) of the input line current. Under the optimal turn ratio, the proposed rectifier operates as an 18-pulse rectifier, with a theoretical THD of input line current of about 10.1 % and an experimental THD of 6.58 %. The proposed method is simple and easy to implement.

The system presented in this study is depicted in Fig. 2 and is structured in two primary stages. The initial stage comprises a three-phase to three-phase matrix converter, while the subsequent stage utilizes a 12-pulse diode rectifier. The primary functions of the matrix converter are twofold: it generates a high-frequency three-phase voltage and meticulously manages the input current to ensure it remains sinusoidal and synchronized with the grid voltage. This precise control significantly reduces harmonics throughout the system, thereby enhancing overall efficiency and stability.

In the second stage, the 12-pulse diode rectifier interfaces directly with the hydrogen electrolyzer, providing the necessary DC power to enable optimal operation and efficient hydrogen production. To achieve robust control of the proposed system, model predictive control (MPC) is implemented. MPC excels in handling multiple variables simultaneously, making it ideal for this application. It is specifically designed to control the amplitude and phase shift of the input current, adjust the frequency and amplitude of the matrix converter output, and maintain a fixed current supply to the hydrogen electrolyzer.

The proposed system merits could be summarized as follows:

- The matrix converter manages input currents to remain sinusoidal and synchronized with the grid voltage, resulting in significant harmonic reduction and improved system efficiency.
- The matrix converter generates a high-frequency three-phase voltage, which contributes to the stability and efficiency of the overall system.
- The 12-pulse diode rectifier provides stable DC power to the hydrogen electrolyzer, ensuring optimal operation and efficient hydrogen production.
- The implementation of model predictive control (MPC) enables sophisticated handling of multiple variables, including the control of input current amplitude and phase shift, and the adjustment of the matrix converter's frequency and amplitude.
- The precise control mechanisms in place ensure overall system stability, even under variable operating conditions.
- The combined use of a matrix converter and a 12-pulse diode rectifier, controlled by MPC, presents a novel and effective power conditioning approach for electrolysis systems.
- The proposed system offers a significant advancement in the integration of renewable energy sources, particularly in enhancing the efficiency and stability of hydrogen production systems.

The remaining structure of the paper are as follows: Section II will delve into the operational principles of the 3-phase matrix converter, detailing its topology, control strategies, and effectiveness in managing input currents while synchronizing with the grid voltage to reduce harmonics and enhance system efficiency. Following this, in Section III, the operation of the 12-pulse rectifier and its interface with the hydrogen electrolyzer will be explored, elucidating its role in providing stable DC power for optimal hydrogen production under variable load conditions. Section IV will elaborate on the control system implemented in the setup, focusing on model predictive control and its multi-variable handling capabilities, crucial for adapting to changing operating conditions. Finally, in Section V, the results of simulations and experiments will be presented and discussed, analyzing system performance, mitigating harmonic distortions, and ensuring stable operation of the hydrogen electrolyzer, while also drawing conclusions and suggesting avenues for future research.

2. 3-phase2 3-phase matric converter operation

The Matrix Converter (MC) stands as a unified power converter

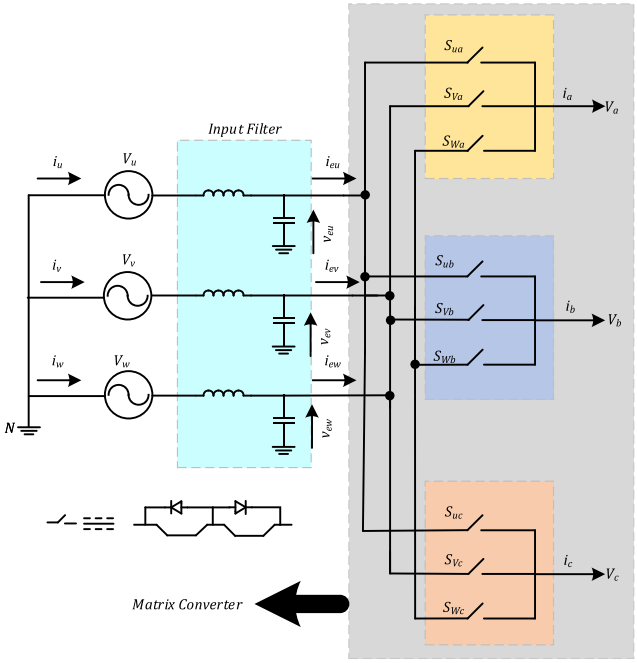

Fig. 3. 3 phase to 3 phase ac-ac matrix converter.

showcasing the ability to directly drive an m-phase load using an n-phase source, without the assistance of energy storage components, typically denoted as an n×m MC ↱ (Blaabjerg et al., 2018). Some of the prominent features that elevate its utility in various sectors include ↱ (Rivera et al., 2017):

- Compact Design: The power circuit design of the MC is space-efficient, making it suitable for installations with spatial constraints.
- High-Quality Power Delivery: The MC can generate superior voltage and current qualities for the load without binding the frequency.
- Efficiency and Harmonic Reduction: MC is known to output sinusoidal input currents, functioning with a unity power factor, thus increasing the efficiency and minimizing harmonic interference.
- Bi-Directional Energy Flow: An exemplary attribute of the MC is its ability to manage energy flow in both directions, from the source to the load and vice-versa. This trait becomes pivotal for applications involving regenerative loads.

A detailed schematic representation of the MC's configuration can be referenced in Fig. 3. This design emphasizes bidirectional switches, ensuring a seamless connection between the three-phase power supply and the three-phase load, leading to a 3×3 MC model. The blueprint in Fig. 3 elucidates the construction of the bidirectional switch, integrating two power transistors paired with their diodes in an anti-series configuration ↱ (Kassas, 2013). An input filter, symbolized by Lf, Rf, and Cf, bridges the MC to the three-phase source. This crucial component serves a dual role ↱ (Vazquez et al., 2019):

- Overvoltage Prevention: It guards the system against potential overvoltages, which might originate from power supply's short-circuit impedance, primarily during the swift commutation of currents like ieu, iev, and iew.
- Harmonic Suppression: The filter efficiently filters out high-frequency harmonics that manifest in input currents, namely iu, iv, and iw, ensuring a harmonious and robust power transmission.

The operational state of each bidirectional switch is represented by a variable, expressed as Sxy, where x∈{u,v,w} and y∈{a,b,c}. The conduction phase of these switches is determined by their respective control

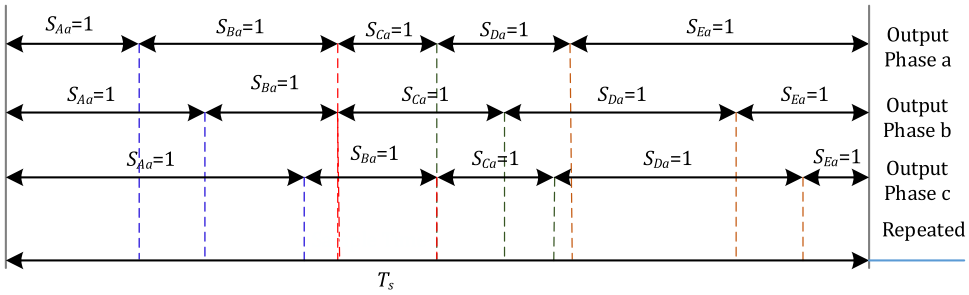

Fig. 4. Matrix converter switching sequence.

signals. For clarity, if Sxy=1, it signals that the switch xy is active, establishing a current passage. However, a value of Sxy=0 implies a deactivated or non-conducting switch.

Given the inductive nature of the loads, it's paramount to ensure the continuity of the load current, mitigating sudden interruptions which might induce overvoltages potent enough to jeopardize system components. Furthermore, it's crucial that the switch operations are orchestrated to avoid short-circuit scenarios between input lines, which could initiate dangerous short-circuit currents. To encapsulate these operational boundaries in a structured mathematical framework, one can establish the following equation

$$S_{uy} + S_{vy} + S_{wy} = 1 \forall y \in \{a, \quad b, \quad c\} \tag{1}$$

The equation describes the relationship between the input and output voltages of a 3×3 matrix converter (MC):

$$\begin{bmatrix} v_a(t) \\ v_b(t) \\ v_c(t) \end{bmatrix} = \begin{bmatrix} S_{ua} & S_{va} & S_{wa} \\ S_{ub} & S_{vb} & S_{wb} \\ S_{uc} & S_{vc} & S_{wc} \end{bmatrix} . \begin{bmatrix} v_{eu}(t) \\ v_{ev}(t) \\ v_{ew}(t) \end{bmatrix} \tag{2}$$

The formula is given using the real-time conversion matrix, symbolized by T. To delineate the input and load voltages in vector form, they can be articulated as follows:

$$V_o = \begin{bmatrix} v_a(t) \\ v_b(t) \\ v_c(t) \end{bmatrix} \tag{3}$$

$$V_i = \begin{bmatrix} v_{eu}(t) \\ v_{ev}(t) \\ v_{ew}(t) \end{bmatrix} \tag{4}$$

By employing the definitions provided in equation (7.3), the relationship between the voltages can be expressed as follows:

$$V_o = T.V_i \tag{5}$$

By applying Kirchhoff's current law to the switches, we can derive the following equation:

$$\begin{bmatrix} i_{eu}(t) \\ i_{ev}(t) \\ i_{ew}(t) \end{bmatrix} = \begin{bmatrix} S_{ua} & S_{va} & S_{wa} \\ S_{ub} & S_{vb} & S_{wb} \\ S_{uc} & S_{vc} & S_{wc} \end{bmatrix} . \begin{bmatrix} i_a(t) \\ i_b(t) \\ i_c(t) \end{bmatrix} \tag{6}$$

Taking into account the current vectors

$$I_i = \begin{bmatrix} i_{eu}(t) \\ i_{ev}(t) \\ i_{ew}(t) \end{bmatrix} \tag{7}$$

$$I_o = \begin{bmatrix} i_a(t) \\ i_b(t) \\ i_c(t) \end{bmatrix} \tag{8}$$

The equation describing the current is as follows:

$$I_i = T^T.I_o \tag{9}$$

The expression T^T denotes the transpose of matrix T.

The two-way switches in the setup function by toggling at an elevated switch rate. This action is orchestrated to yield a voltage of lower frequency that boasts modifiable amplitude and frequency. This voltage waveform's creation is realized using switch blueprints, as illustrated in ↱Fig. 4. In essence, the load voltage's low-frequency facet is formulated by intermittently capturing the input voltages and suitably actuating the bidirectional switches.

To meticulously determine the time span for which each switch Sij stays activated (ON), symbolized as tij, and taking T as the sampling time frame, the load voltage's low-frequency facet can be detailed as follows:

$$\overline{v}_{jn}(t) = \frac{t_{uj}.v_{eu}(t) + t_{vj}.v_{ev}(t) + t_{wj}.v_{ew}(t)}{T} j \in \{a, \quad b, \quad c\} \tag{10}$$

The low-frequency component $\overline{v}_{jn}(t)$ represents the mean value calculated over a single sampling interval T of the output phase j. From an examination of Figure 7.2, it's evident that the voltage corresponding to phase a arises by supplying the load voltage veu within the time frame tua, the voltage vev within the interval tva, and the voltage vew during the duration twa.

Nevertheless, it's imperative to guarantee that the activation durations of the switches adhere to specific boundaries.

$$T = t_{uj} + t_{vj} + t_{wj} \forall j \in \{a, \quad b, \quad c\} \tag{11}$$

By establishing the duty cycles as

$$m_{uj}(t) = \frac{t_{uj}}{T}, \quad m_{vj}(t) = \frac{t_{vj}}{T}, \quad m_{wj}(t) = \frac{t_{wj}}{T} \tag{12}$$

By defining the duty cycles as mentioned earlier and then expanding equation (7.8) for each phase, we arrive at the following set of equations:

$$\begin{bmatrix} \overline{v}_{aN} \\ \overline{v}_{bN} \\ \overline{v}_{cN} \end{bmatrix} = \begin{bmatrix} m_{ua} & m_{va} & m_{wa} \\ m_{ub} & m_{vb} & m_{wb} \\ m_{uc} & m_{vc} & m_{wc} \end{bmatrix} . \begin{bmatrix} v_{eu} \\ v_{ev} \\ v_{ew} \end{bmatrix} \tag{13}$$

$$\overline{V}_o = \begin{bmatrix} \overline{v}_{aN} \\ \overline{v}_{bN} \\ \overline{v}_{cN} \end{bmatrix} \tag{14}$$

$$\overline{V}_o = M(t).v_i(t) \tag{15}$$

In this context, we have the low-frequency output voltage vector denoted as $\overline{V}_o$, the instantaneous input voltage vector represented as $v_i(t)$, and the low-frequency transfer matrix of the MC, denoted as M(t).

Following a similar approach for the input currents, it can be shown that

$$\overline{i}_i(t) = M^T(t).i_o(t) \tag{16}$$

In this context, the low-frequency component of the input current vector is represented as $\overline{i}_i(t)$, and the transpose of the matrix M(t) is denoted as $M^T(t)$.

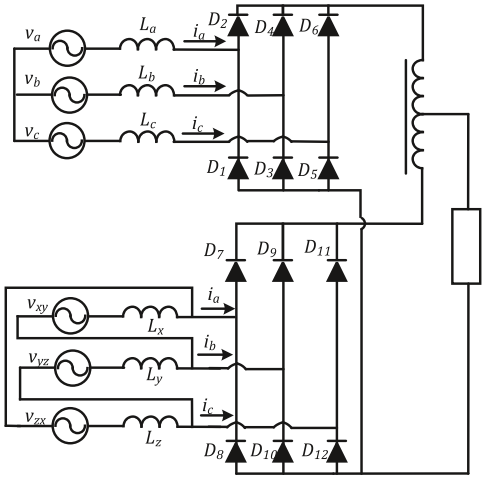

Fig. 5. 12-pulse bridge rectifier.

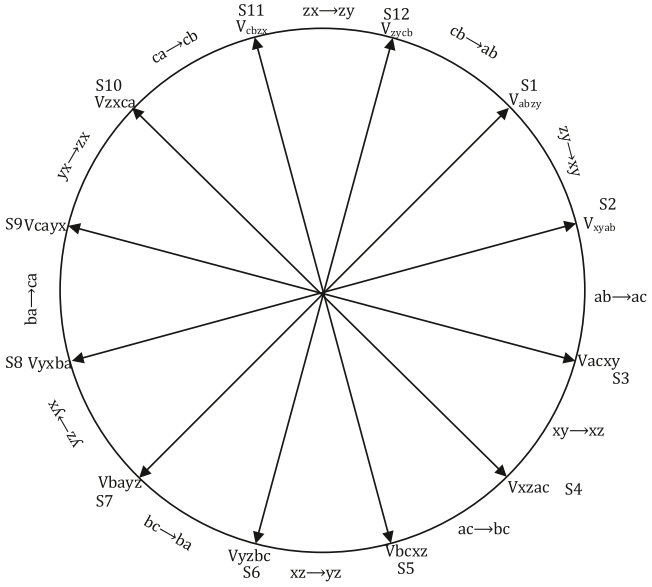

Fig. 6. A comprehensive 12-pulse vector diagram.

3. 12 Pulse rectifier operation

The structure shown in ↱Fig. 5 showcases a 12-pulse diode rectifier, integrating two distinct 6-pulse diode bridge rectifiers arranged in series ↱ (Rodriguez and Cortes, 2012; Bayhan et al., 2018). This rectifier draws power from two independent 3-phase secondary transformers. One of these transformers adopts a star linkage, while the other employs a delta pattern. The voltage metrics for both these secondary transformers can be articulated as per Eqs. (1–6).

$$v_a = V_a.\sin(wt - \varphi_a) \tag{17}$$

$$v_b = V_b.\sin(wt - \frac{2\pi}{3} - \varphi_a) \tag{18}$$

$$v_c = V_c.\sin(wt + \frac{2\pi}{3} - \varphi_a) \tag{19}$$

$$v_{xy} = V_{xy}.\sin(wt - \varphi_{xy}) \tag{20}$$

$$v_{yz} = V_{yz}.\sin(wt - \frac{2\pi}{3} - \varphi_a) \tag{21}$$

Table 1
Comparative Analysis of 12-Pulse Diode Rectifier Topologies. *NR___Not reported analysis.

Topology	Efficiency	PF	THD	Components
12-pulse rectifier with conventional transformer unit (CTU). ↱[84]	< 97 %	0.88	< 8 %	12 Diodes + CTU
12-pulse rectifier with autotransformer unit (ATU). [84]	< 98 %	0.82	< 2 %	12 Diodes + ATU
12-pulse rectifier with three level choppers. ↱[77]	<97.5 %	0.975	2 %–5 %	15 Diodes + 3 Mosfets
12-pulse rectifier based on retrofit polygon autotransformer + Pulse tripling circuit (PTC). ↱[85]	97.95 %	0.99	1.03 %	12 Diodes + Polygon ATU + PTC
Proposed 12-Pulse Diode Rectifier with Pulse Multiplication circuit (PMC). ↱[83]	NR	NR	0.7 %	12 Diodes + polygon ATU + PMC

$$v_{zx} = V_{zx}.\sin(wt + \frac{2\pi}{3} - \varphi_a) \tag{22}$$

Where v_a=v_b=v_c=V_m (Phase magnitude)

$$v_{xy} = v_{yz} = v_{zx} = \sqrt{3}V_m \tag{23}$$

A comprehensive representation of the potential conducting states for a 12-pulse diode bridge rectifier, highlighting the intricate dynamics introduced by the commutation angle, denoted as μ is illustrated in ↱Fig. 6. This angle is pivotal in representing the overlap duration, a phenomenon induced primarily by the inherent supply and load inductances in the diode bridge structure. During this period, the rapid transition of current across the diode phases is inhibited, thereby affecting the operational states of the rectifier.

In scenarios where diodes are interconnected to sources with augmented reactance, the overlap duration inherent to the rectifier might be extended. Consequently, this can usher the system into more intricate operational states. Systematically categorizing these states based on the overlap angle, we can identify three distinct operational modes:

Overlap Mode 1(0≤μ<60◦): This mode encapsulates the operational dynamics where the commutation overlap angle μ remains less than 60 degrees. Functionally, the bridge operates conventionally within this mode. Throughout the overlap period, the diode count oscillating between active states can fluctuate between two and three.

Overlap Mode 2(μ=60◦): A subsequent elevation in the supply inductance can transition the system to this mode. Here, the commutation overlap angle μ stabilizes at a consistent 60 degrees. Intrinsically, during this mode, a trio of diodes remain actively conducting, manifesting a stability in the system's dynamics.

Overlap Mode 3(μ>60◦): Amplifying the AC input inductance further evolves the bridge circuitry to this mode. Herein, the overlap angle μ exceeds the 60-degree threshold. The peculiarity of this mode is the initiation of overlap even before the culmination of the preceding commutation. Within this operational envelope, the device count oscillating between active states is not rigid and can waver between three and four.

Connecting the theoretical understanding with the provided figure, it's discernible that the sectors, notably S1 to S47, possibly delineate the various conducting states of the diode bridge. Transitions between these sectors capture the essence of the current flow and the intertwined effects of commutation. The triad of dominant directions (namely x, y, and z) embedded in the diagram can be postulated to represent the three inherent phases of the 12-pulse bridge. Furthermore, the interspersed transitions might signify the metamorphosis from one state to its

successor, undrpinned by the varying overlap conditions and their corresponding operational modes.

Table 1 illustrates how the performance of 12-Pulse rectifiers varies based on factors such as converter complexity, filter types, and phase shift transformer designs. Utilizing a Conventional Transformer Unit (CTU) results in the lowest efficiency, power factor (PF), and highest Total Harmonic Distortion (THD %). Replacing CTU with an Autotransformer Unit (ATU) enhances efficiency but yields the lowest PF and reduced THD. Integrating an interleaved buck converter with CTU significantly improves efficiency, achieves satisfactory PF, and maintains natural THD %. Incorporating a pulse tripling circuit elevates efficiency, delivers excellent PF, and ensures superior THD. Additionally, implementing a pulse multiplication circuit within the rectifier can further refine THD levels.

4. Control system operation

Model Predictive Control (MPC), an avant-garde control strategy, emerges as the nexus between optimal control theory and real-time decision-making. At its core, MPC revolves around leveraging an explicit model of the system, formulating an optimization problem, and then determining the optimal control inputs over a stipulated horizon. The principle that underpins MPC is forecasting: it anticipates future events and orchestrates responses proactively. In every iteration, MPC evaluates the system's predicted behavior over a defined prediction horizon and optimizes the control inputs to minimize a certain cost function, which typically encompasses setpoint tracking and control effort. Post optimization, only the first control move is applied, after which the process is reiterated with updated measurements ↱ (Singh et al., 2010; Zhaksylyk et al., 2023; Liserre et al., 2005; Guo et al., 2014; Garcia et al., 2017).

The merits of MPC are manifold. Foremost, its ability to handle multi-input multi-output (MIMO) systems effortlessly sets it apart from its contemporaries. Moreover, constraints, a quintessential feature of real-world systems, are inherently embraced within the MPC framework, ensuring that the system always operates within safe and predefined boundaries. MPC's foresight also imparts a natural resilience against disturbances, both measured and unmeasured. Another compelling facet is its compatibility with nonlinear models, thus bridging the often-wide chasm between real-world systems and their linear counterparts.

4.1. Load representation

In the given context, the overarching objective is to formulate an equation capable of predicting the upcoming sampling interval's load current value across all the switching states. The load current equation could be formulated as follows:

$$L\frac{di_o(t)}{dt} = V_o(t) - RI_o(t) \tag{24}$$

The presented formula embodies a load model characterized by the parameters L and R, which denote the load's inductance and resistance, respectively.

Furthermore, it's pivotal to acknowledge the estimated value for the output current's derivative. This estimation plays a cardinal role as it paves the way for streamlined computations of the load model's dynamic behavior. Through this approximation, practitioners and researchers are positioned to delve deep into the intricacies of the load's dynamics, crafting adept control methodologies that elevate system efficacy. Such depth in modeling and scrutiny fosters the inception of avant-garde solutions spanning a range of industrial and technological arenas.

$$\frac{dI_o}{dt} \approx \frac{I_o(k+1) - I_o(k)}{T_S} \tag{25}$$

Considering the sampling duration Ts, we can extrapolate the equation to anticipate the load current by integrating Eq. (24) into Eq. (25). This derivation produces a model capable of forecasting the load current's trajectory within a specified sampling time frame. The resultant formula captures the load's dynamic response influenced by multiple determinants, such as the sampling duration and associated parameters. This foresight is paramount in control systems and engineering domains, facilitating agile decision processes and on-the-fly adaptations for peak operational efficiency. By grasping and applying this forecasting model, professionals can bolster system robustness and agility, ensuring they remain receptive to evolving conditions and unexpected variables. These prognostic techniques are pivotal, driving technological progression and bolstering dependability and productivity in a spectrum of industrial sectors.

$$I_o(k+1) = \left(1 - \frac{RT_S}{L}\right)I_o(k) + \frac{T_S}{L}(V_o(k)) \tag{26}$$

The formula aims to predict the upcoming load current, io(k + 1), for the next sampling phase (k + 1), taking into account various load voltage readings, vo(k). By analyzing the load voltage array, vo(k), in relation to the 27 possible converter switching states, professionals can gauge how the load current might change in the forthcoming period.

Using this anticipatory method, both engineers and control mechanisms can effectively anticipate and manage load variations. With the help of reliable forecasting tools and methodologies, systems can actively adapt to changes, ensuring consistent performance. This level of accuracy and adaptability is crucial in multiple areas, such as motor drive applications, energy conversion units, and grid-connected setups.

4.2. Input filter model

The input filter model, derived from the circuit depicted in ↱Fig. 3, can be characterized by a set of continuous-time equations:

$$V_S(t) = R_f I_S(t) + L_f\frac{dI_s(t)}{dt} + V_i(t) \tag{27}$$

$$I_S(t) = I_i(t) + C_f\frac{dV_i(t)}{dt} \tag{28}$$

The mathematical model captures the intricacies of the line and filter system through its key parameters: Lf, Rf, and Cf. These elements — the inductance (Lf), resistance (Rf), and capacitance (Cf) — serve as the pillars that dictate the operational characteristics of the system.

Lf, the inductance, is pivotal in deciding how swiftly the current through the system can change. A higher inductance typically restricts rapid current variations, making it beneficial in scenarios where steady current flow is desired. The resistance, denoted as Rf, is the measure of how much energy is dissipated as heat in the system. It acts as a dampening agent, reducing oscillations and preventing possible system instabilities. On the other hand, the capacitance, Cf, is crucial for stabilizing voltage fluctuations. It acts as a reservoir, absorbing and releasing energy, thereby mitigating abrupt voltage changes.

For professionals working in the realm of electronics and power systems, decoding the interplay between these parameters is indispensable. This knowledge is instrumental in ensuring that the line and filter system operates at its peak efficiency, minimizes energy losses, and stands robust against potential disturbances.

In essence, the choice of Lf, Rf, and Cf isn't arbitrary. It's a meticulous decision, grounded in the understanding of system requirements and the desired outcomes. Whether it's curbing interference in communication systems or ensuring smooth power delivery in electric grids, the tailored design of these parameters is what makes the difference. This mathematical model serves as a compass, guiding engineers in the intricate journey of system optimization and refinement.

$$V_S(t) = 2/3\left(v_u + av_v + a^2v_w\right) \tag{29}$$

$$I_S(t) = 2/3\left(I_u + aI_v + a^2 I_w\right) \tag{30}$$

The present system operating in continuous-time can be reformulated as follows:

$$\dot{X}(t) = \begin{bmatrix} V_i(t) \\ i_s(t) \end{bmatrix} \text{and} u(t) = \begin{bmatrix} V_S(t) \\ i_i(t) \end{bmatrix} \tag{31}$$

When implementing a zero-order hold input on a continuous-time system represented in state space form, it leads to the derivation of a discrete state space model. By introducing a sampling period Ts, we can transform the continuous-time system described in Eq. (24) into a discrete-time system, yielding the following representation:

$$X(k+1) = A_q X(k) + B_q u(k) \tag{32}$$

with

$$A_q = e^{A_C T_S} \text{and} B_q = \int_0^{T_S} e^{A_C(T_S-\tau)} B_c d\tau \tag{33}$$

The transition from a continuous-time system to a discrete-time system is crucial in the digital control of systems. The sampled-data approach enables engineers and researchers to deploy digital controllers for systems originally represented in continuous-time.

MATLAB c2d() function acts as an invaluable tool in this transition. By effectively converting the continuous-time model to its discrete counterpart, it facilitates the implementation and simulation of control strategies that work on digital platforms. Given the ubiquity of digital control systems in today's world, from industrial applications to consumer electronics, this transition is more relevant than ever.

Equation (7.29), as referenced, is crucial for predicting the mains current. Predictive control, as its name suggests, is all about forecasting the future states of a system and adjusting the inputs accordingly to achieve desired performance criteria. By predicting the behavior of the mains current, engineers can make proactive decisions, preventing issues before they arise, leading to smoother operations and enhanced reliability.

The combination of theory, predictive modeling, and powerful computational tools such as MATLAB provides a holistic approach to system analysis and control. It merges the rigorous mathematical foundation with the practical ease of simulation and implementation. Thus, engineers are not only equipped with the tools to design and analyze systems but also to visualize, simulate, and test their strategies in a virtual environment before actual deployment. This synergy of theory and practical tools paves the way for innovations and advancements in the realm of control systems and their applications.

$$i_s(k+1) = A_q(2,1)v_e(k) + A_q(2,2)i_s(k) + B_q(2,1)v_s(k) + B_q(2,2)i_e(k) \tag{34}$$

At this stage, the approach can employ the obtained model to forecast the value of is based on the input parameter ii. Subsequently, Eq. (34) is utilized to calculate ii for every switching state.

4.3. Real-time reactive power fluctuations

Enhancing the performance of the system is to control the reactive power generated from the wind by adjusting the phase-shift between the input voltage and current. The calculation of this reactive power is achieved through the utilization of the following equation (Mazloomi and Sulaiman, 2012).

$$Q = IM\{V_S(t).\bar{I}_S(t)\} \tag{35}$$

The equation involves the extraction of the imaginary part of the product of the vectors, and $\bar{I}_S(t)$ represents the complex conjugate of is Is (t). Predicting the instantaneous reactive power can be achieved through the implementation of.

$$\begin{aligned} Q(k+1) &= IM\{V_S(k+1).\bar{I}_S(k+1)\} \\ &= v_{s\beta}(k+1)i_{s\alpha}(k+1) - v_{s\alpha}(k+1)i_{s\beta}(k+1) \end{aligned} \tag{36}$$

The subscripts α and β denote the real and imaginary elements of the corresponding vector. The estimation for the future value of the input current, is(k + 1), is derived from Eq. (34).

Regarding the line voltages, they are characterized as low-frequency signals, allowing us to approximate vs(k + 1) to be approximately equal to vs(k).

4.4. Control of output current while reducing input reactive power

The magnitude of this input current is inherently tied to the active power flow, given that the MC doesn't possess energy storage capabilities. Targeting a unity power factor often necessitates the adoption of sophisticated strategies, as evident in many modulation techniques. Yet, when the goal is to function with either inductive or capacitive power factors, the intricacy of the challenge escalates notably.

However, the introduction of the predictive control paradigm offers a silver lining. It presents an efficient mechanism for managing the reactive power, Q. This effectiveness stems from the ability to discern and subsequently penalize those switching states that prompt predictions of Q that veer too far from the set reference value. Hence, predictive control paves the way to seamlessly meet the specified reactive power control goals, sidestepping the complexities that traditional methods might introduce.

$$g_2 = |Q^* - Q^P(k+1)| \tag{37}$$

For each appropriate switching state, the predicted reactive power, Qp, is derived from Eq. (36). The set reference value, Q*, indicates if the system operates with capacitive, inductive, or a unity power factor (PF). In numerous scenarios, a unity PF is preferred, meaning Q* = 0 and g2 = |Qp|. Nonetheless, this technique offers *a* more direct control option for this parameter compared to other modulation methods.

To fulfill both goals – controlling output current and reactive input power – a combined cost function is formed by merely summing g1 and g2. This method allows for the proficient oversight of system efficacy, effectively achieving the targeted power factor control along with optimal output current stability. Using this integrated cost function, professionals can conveniently calibrate and modify control settings, making it easier to enhance system efficiency across various real-world applications.

$$g = \left|i^*_{o\alpha} - i^P_{o\alpha}\right| + \left|i^*_{o\beta} - i^P_{o\beta}\right| + A\left|Q^* - Q^P\right| \tag{38}$$

The weighing factor, A, acts as the backbone in the decision-making process within the predictive control strategy. It essentially provides a scalar value, quantifying the significance or priority of different objectives within the control system. Considering that the terms in the cost function, g, can span across various units, having A with a unit of V^(-1) provides a standardized metric to balance these terms.

The dynamic nature of A is what sets this control scheme apart. Its value is not rigid; it's adjustable. This means that the system can pivot its focus between two significant objectives: maintaining the power factor (or managing reactive input power) and adhering to the output current reference tracking. By dialing up the value of A, the system becomes more inclined to maintain the desired power factor, ensuring that the power system operates efficiently and reduces potential power losses. Conversely, reducing A's value shifts the controller's attention towards closely tracking the output current reference, ensuring the system output aligns with the desired target.

This tunability offers a notable advantage. It's not a one-size-fits-all solution; the control system can be calibrated according to the specific needs of a given application. Whether the emphasis is on power quality, energy efficiency, or precise output tracking, by simply adjusting the

Table 2
System simulation parameters.

Parameter	Description
Operating Voltage:	Minimum: 20 V Maximum: 25 V Optimal: 24 V
Operating Current:	Maximum: 30 A
Inputs	3-phase, 440 V, 50 Hz
LF	900 uH
Cf	600 μF
Ts	10 us

weighing factor A, the control system can be fine-tuned to prioritize different objectives. This dynamic approach not only ensures optimal system performance but also paves the way for adaptable solutions in an ever-evolving technological landscape.

5. Results

To validate the functionality of the proposed system, we conducted a comprehensive simulation using MATLAB Simulink under the operational conditions outlined in Table 2. The increasing emphasis on integrating renewable energy sources into contemporary energy systems necessitates rigorous evaluations to ensure optimal performance. Notably, wind energy is a significant focus in this paradigm shift, a fact accentuated by the system demonstrated in this research. The three-phase generator connected to the wind turbine, depicted in Fig. 7, epitomizes sustainable energy capture. This configuration is distinguished not only by its eco-friendly approach to power generation but also by its sophisticated design, ensuring system stability amidst variable wind conditions. The gearbox plays a crucial role in maintaining a uniform generator speed regardless of wind speed variability, which is pivotal for consistent energy production. The system delivers a 311 V/50 Hz sinusoidal voltage, signaling a viable pathway for energy systems that require stability, especially in regions with volatile wind patterns. The voltage amplitude oscillates between −400 V and 400 V over a time span from approximately 0.085 seconds to 0.115 seconds. Three distinct sinusoidal outputs are observed: Va(in) in blue representing phase one, Vb(in) in orange for phase two, and Vc(in) in yellow for phase three. The phase shifts among these waveforms highlight the balanced nature of the three-phase AC system, with evenly distributed peaks underscoring its inherent equilibrium.

Examining harmonic distortions reveals the dual nature of sinusoidal currents in such configurations. While an ideal sinusoidal waveform enhances energy transmission efficiency and reduces losses, achieving this amid power electronic switches remains challenging, as evidenced in existing literature. Fig. 8's depiction of the input current from the proposed topology suggests potential advancements in this domain. However, the system's ability to regulate both the output voltage and current for the hydrogen electrolyzer while shaping the input current is its most significant feature. Fig. 9's harmonic content and subsequent analysis provide critical proof of the system's proficiency in handling these challenges, indicating the viability of renewable energy-focused configurations in practical implementations. The introduction of the LC filter subsequent to the wind generator's terminal is a cornerstone of the design blueprint. The significance of such a filter, particularly within the renewable energy sphere, is paramount. The post-filter voltage and current profiles, represented in Figs. 10 and 11, underline this component's crucial function. Even minor harmonic distortions can lead to system inefficiencies, and the LC filter's integration proactively counters such potential issues, fortifying power transmission quality.

Matrix converters, known for their dynamic capabilities, impart the system with unparalleled versatility. Their adeptness at modulating both amplitude and frequency makes the system adaptable, as depicted in Figs. 12 and 13. Analyzing the system's frequency-responsive behavior provides insights into its robustness and adaptability, essential for applications where energy source variations and end-use system requirements are intertwined, exemplified by the hydrogen electrolyzer. The performance of the hydrogen electrolyzer remains central to this research. Its operational prerequisites, particularly the unyielding 24 V voltage for optimal functioning, are stringent. Observations from Fig. 14, which highlight the stable electrolyzer voltage despite current perturbations, are paramount. These findings denote a robust system design capable of insulating end-use components from upstream irregularities, ensuring uninterrupted hydrogen generation.

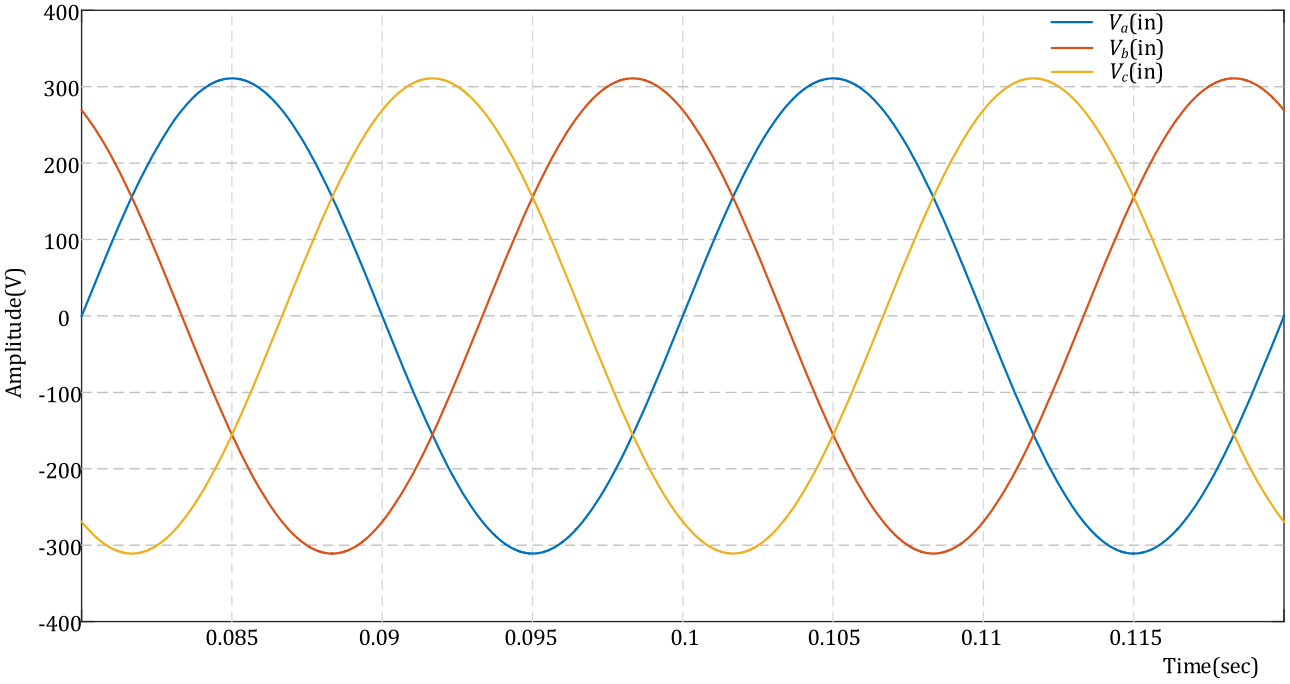

Fig. 7. Three-phase input voltage.

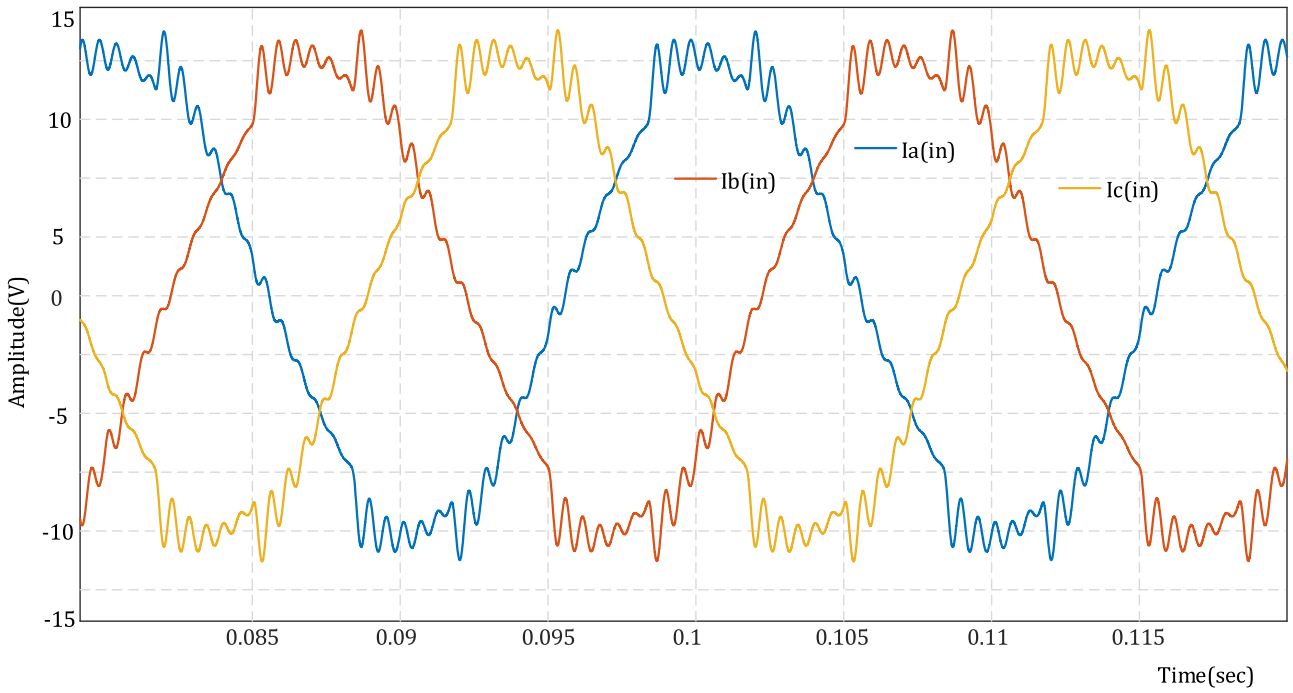

Fig. 8. Three-phase input current.

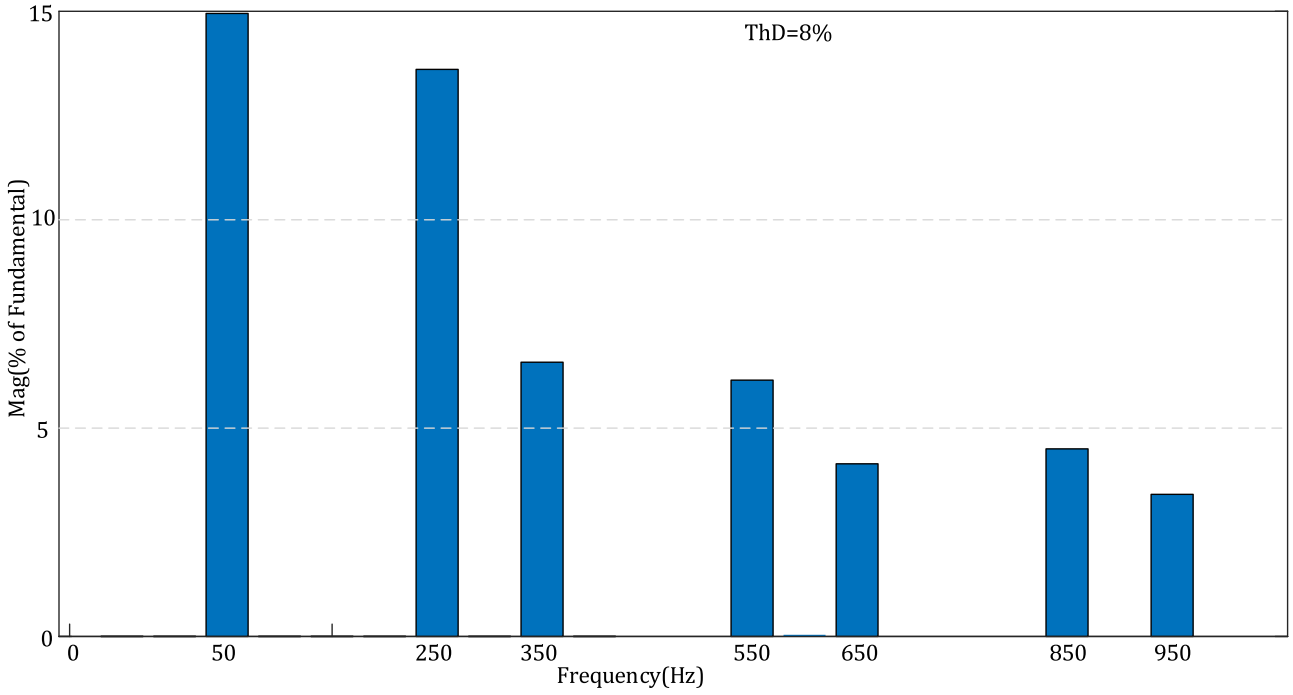

Fig. 9. Total harmonic distortion of the input current.

6. Conclusion

The system described in Fig. 2 comprises two main components: an initial matrix converter followed by a 12-pulse diode rectifier. The matrix converter effectively manages the input current, ensuring synchronization with the grid voltage, which significantly reduces harmonics and enhances overall system efficiency. The 12-pulse diode rectifier directly interfaces with the hydrogen electrolyzer, providing the necessary DC power for optimal hydrogen production. Through the integration of model predictive control, the system demonstrates exceptional multi-variable handling capabilities. Validations conducted using MATLAB Simulink simulations confirm the operational viability of the proposed system. Within the context of renewable energy integration, wind energy, as demonstrated by the capture mechanism in Fig. 7, emerges as a key contributor. The system's resilience, particularly in coping with wind speed fluctuations, highlights the robustness of its design. Harmonic distortions present significant challenges, yet the proposed topology offers a compelling solution. Figs. 8 and 9 illustrate the harmonic analysis, showcasing the system's proficiency in addressing these challenges and signaling a promising future for renewable-

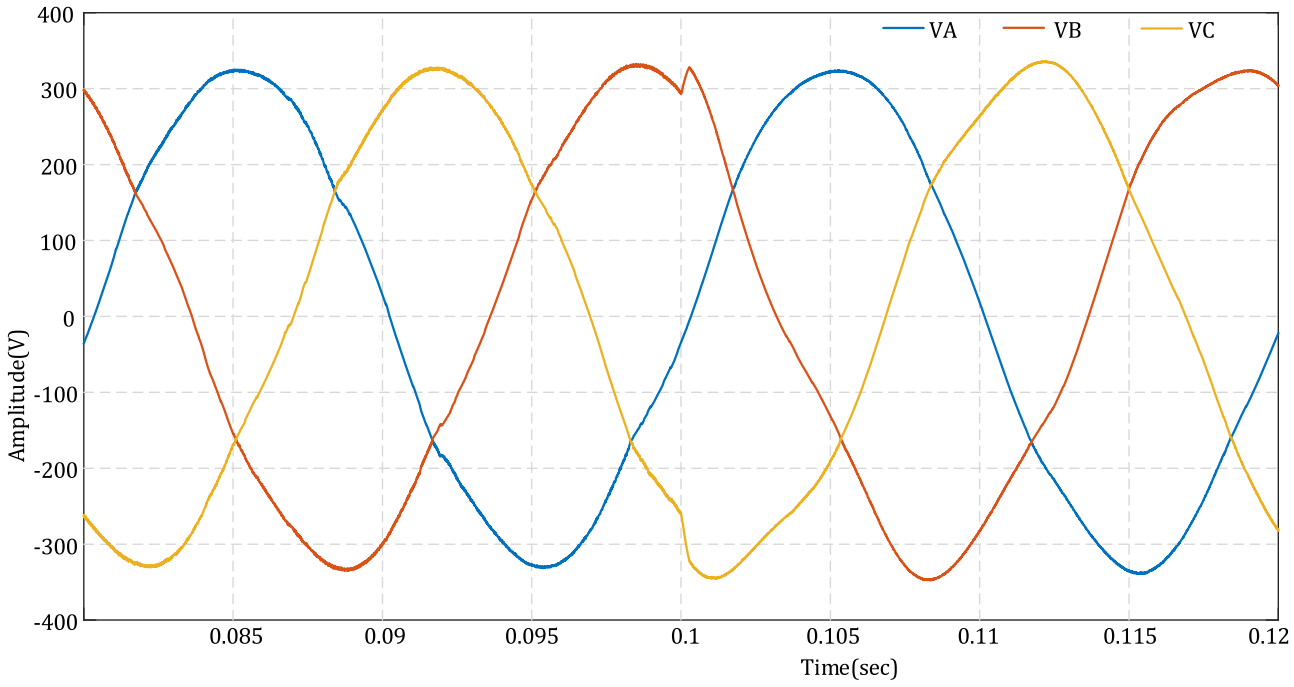

Fig. 10. Three-phase voltage after the filter.

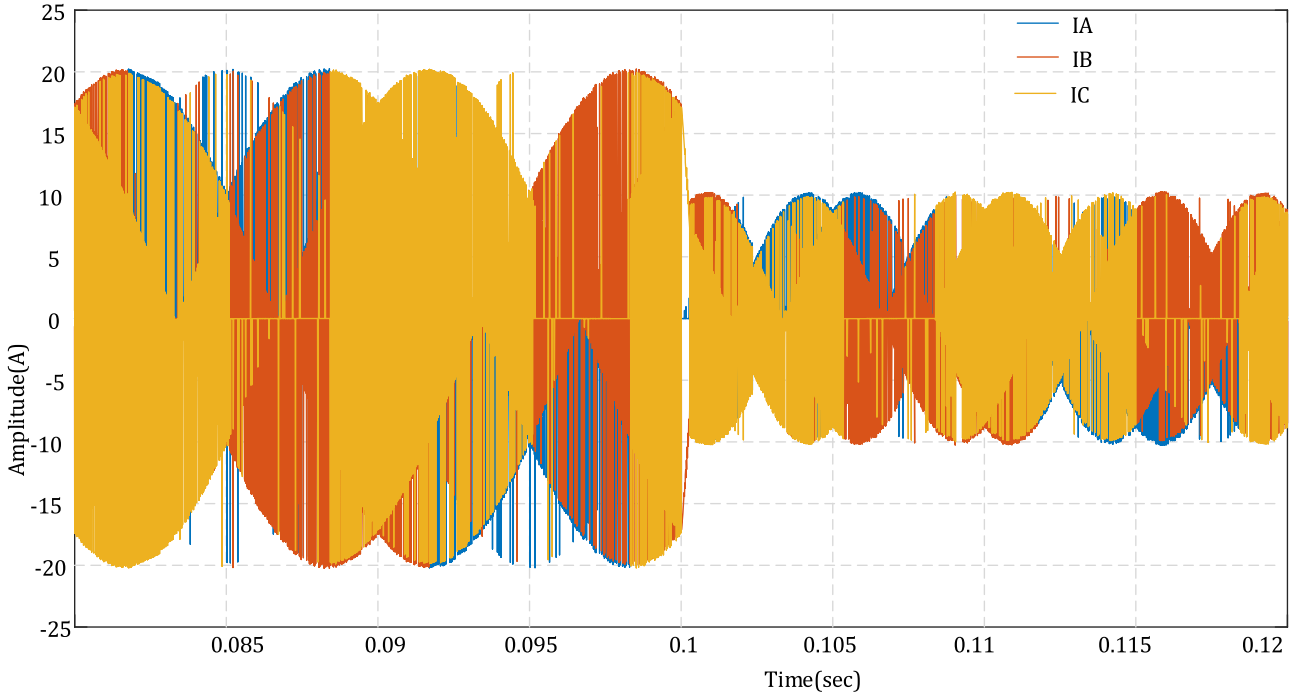

Fig. 11. Three-phase current after the filter.

focused systems. The strategic inclusion of the LC filter enhances the system's resistance to potential inefficiencies caused by harmonic distortions. The dynamic capabilities of matrix converters, as depicted in Figs. 12 and 13, highlight the system's adaptability, which is especially important when examining the performance metrics of the hydrogen electrolyzer. Observations in Fig. 14 emphasize a robust system architecture that remains insulated against potential upstream perturbations, ensuring consistent hydrogen generation.

Author statement

We are pleased to inform you that we have thoroughly addressed all the issues and suggestions raised by the reviewers. We have diligently revised the manuscript to ensure that every point is comprehensively addressed. Our detailed response includes a comprehensive outline of all changes made and suitable rebuttals for any comments that could not be fully addressed.

Please be assured that we have dedicated ourselves to enhancing the quality and clarity of our manuscript in alignment with the reviewers'

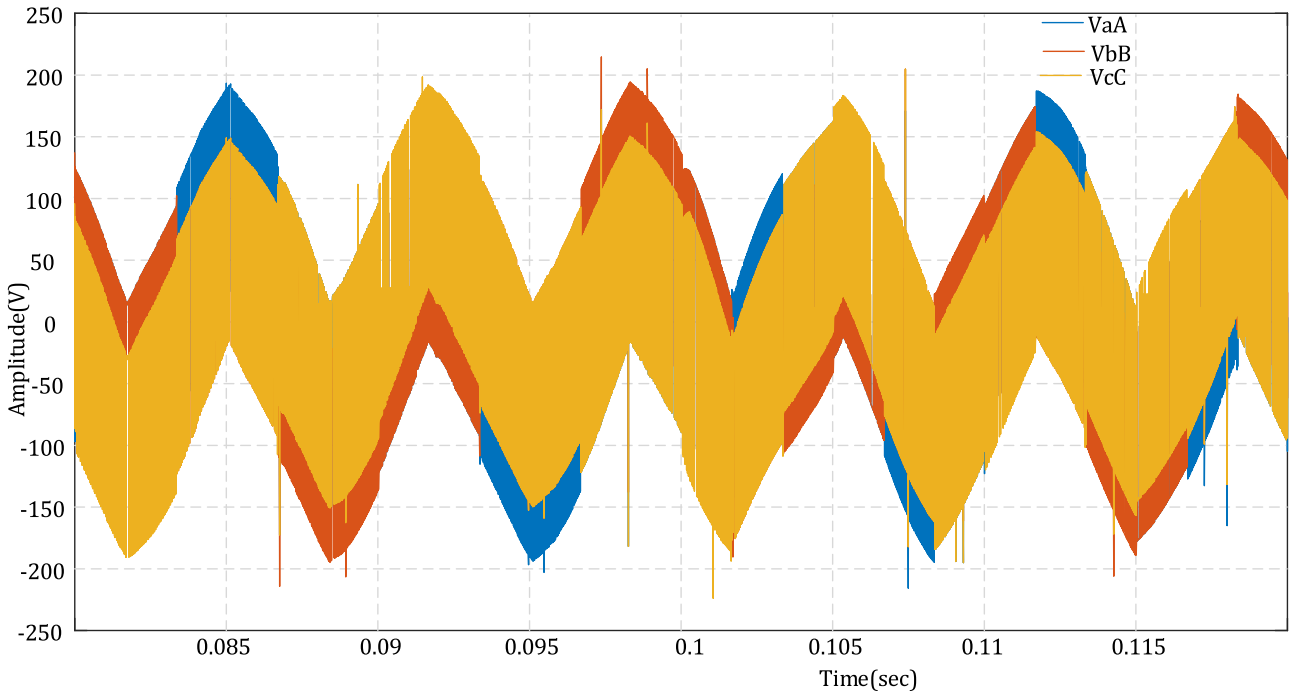

Fig. 12. Three-phase voltage at the output terminal of the matrix converter.

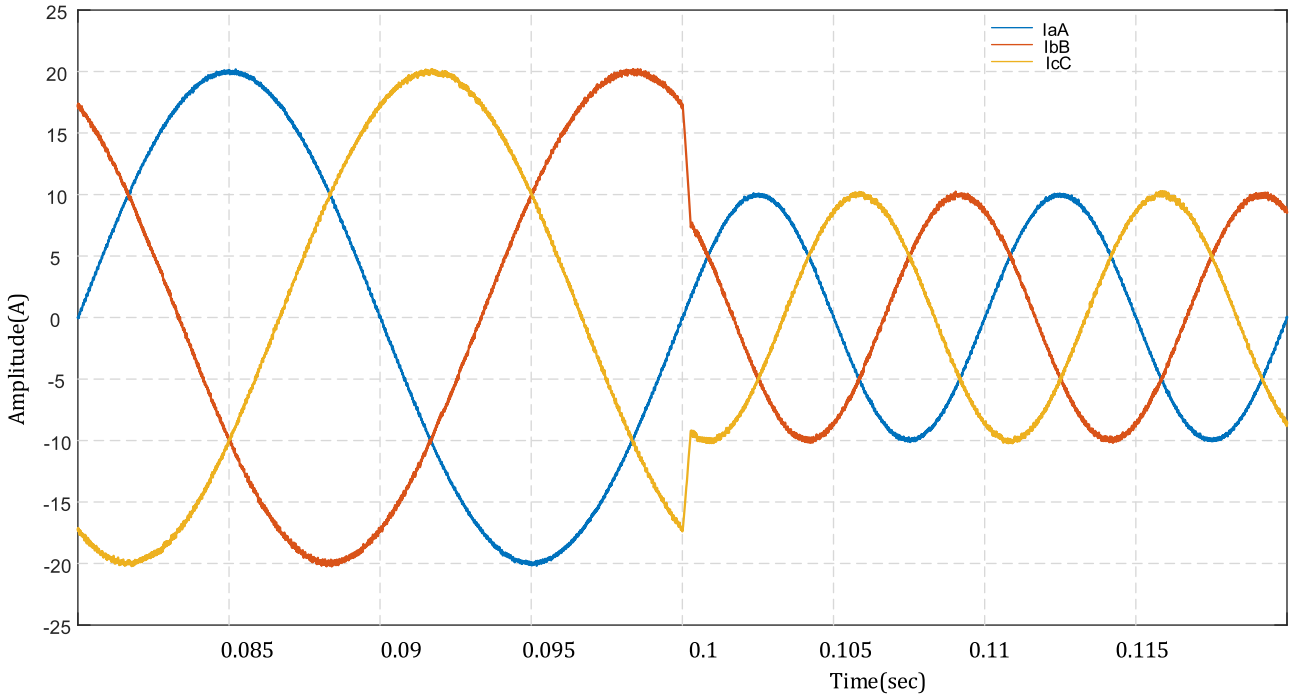

Fig. 13. Three-phase current at the output terminal of the matrix converter.

expectations. We have carefully considered each comment to improve the robustness and scientific merit of our work.

We are confident that the revisions have substantially improved the manuscript and have addressed the reviewers' concerns comprehensively.

CRediT authorship contribution statement

Thamer A. H. Alghamdi: Writing – review & editing, Funding acquisition. **Adel B Abdel-Rahman:** Writing – original draft, Methodology. **Omar Abdel-Rahim:** Writing – review & editing, Writing – original draft, Validation, Software, Resources, Methodology, Investigation, Formal analysis, Data curation, Conceptualization. **Wesam Rohouma:** Writing – review & editing, Resources, Methodology, Funding acquisition.

Declaration of Competing Interest

The authors declare that they have no known competing financial interests or personal relationships that could have appeared to influence

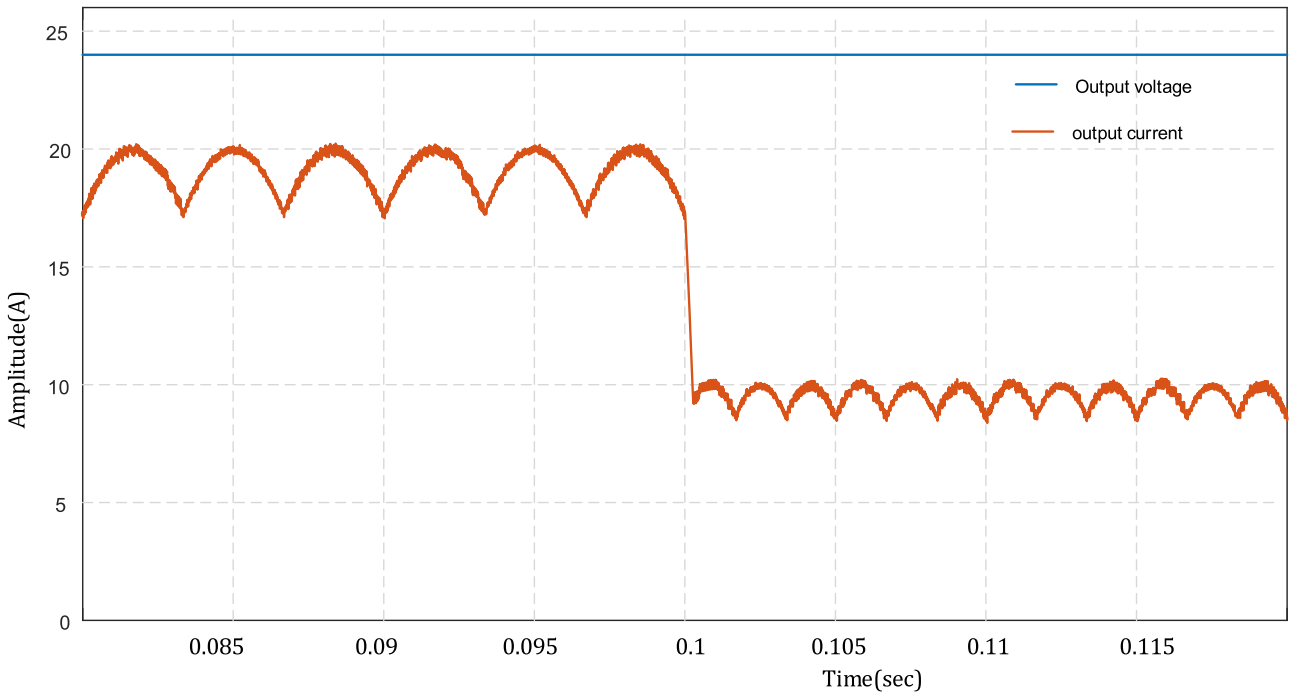

Fig. 14. Voltage and current applied to the hydrogen electrolyser.

the work reported in this paper.

Data availability

Data will be made available on request.

References

Abdollahi, R., Gharehpetian, G.B., Anvari-Moghaddam, A., Blaabjerg, F., 2021. Pulse tripling circuit and twelve pulse rectifier combination for sinusoidal input current. IEEE Access vol. 9, 103588–103599. https://doi.org/10.1109/ACCESS.2021.3098620.

Sertac Bayhan, Panagiotis Kakosimos, Marco Rivera. Predictive torque control of brushless doubly fed induction generator fed by a matrix converter, 2018 IEEE 12th International Conference on Compatibility, Power Electronics and Power Engineering (CPE-POWERENG 2018), 2018.

Blaabjerg, F., Yang, Y., Ma, K., 2018. Power electronics - the key technology for renewable energy systems. Proc. IEEE 106 (12), 2077–2090.

Brouwer, Jacob, 2010. On the role of fuel cells and hydrogen in a more sustainable and renewable energy future (Supplement). Curr. Appl. Phys. Volume 10 (Issue 2), S9–S17.

Buttler, A., Spliethoff, H., 2018. Current status of water electrolysis for energy storage, grid balancing and sector coupling via power-to-gas and power-to-liquids: a review. Renew. Sustain. Energy Rev. 82, 2440–2454.

Carmo, M., Fritz, D.L., Mergel, J., Stolten, D., 2013. A comprehensive review on PEM water electrolysis. Int. J. Hydrog. Energy 38 (12), 4901–4934.

De Lorenzo, Giuseppe, Agostino, Raffaele Giuseppe, Fragiacomo, Petronilla, 2022. Dynamic electric simulation model of a proton exchange membrane electrolyzer system for hydrogen production. Energies 15 (17), 6437. https://doi.org/10.3390/en15176437.

Du, Qingxiao, Gao, Lei, Li, Quanhui, Liu, Wei, Yin, Xinyu, Meng, Fangang, 2022a. Harmonic reduction methods at DC link of series-connected multi-pulse rectifiers: a review. IEEE Trans. Power Electron.

Du, Q., Gao, L., Li, Q., Liu, W., Yin, X., Meng, F., 2022b. Harmonic reduction methods at DC link of series-connected multi-pulse rectifiers: a review (March). IEEE Trans. Power Electron. vol. 37 (3), 3143–3160. https://doi.org/10.1109/TPEL.2021.3118040.

Garcia, Cristian F., Rivera, Marco E., Rodriguez, Jose R., Wheeler, Pat W., Pena, Ruben S., 2017. Predictive current control with instantaneous reactive power minimization for a four-leg indirect matrix converter. IEEE Trans. Ind. Electron.

Guo, Xiaoqiang, Zhang, Xue, Wang, Baocheng, Wu, Weiyang, Guerrero, Josep M., 2014. Asymmetrical grid fault ride-through strategy of three-phase grid-connected inverter considering network impedance impact in low-voltage grid. IEEE Trans. Power Electron.

Kassas, Mahmoud, 2013. Analysis of 12-pulse rectifier operation under balanced and unbalanced voltage source with input impedance. Arab. J. Sci. Eng.

Liserre, M., Blaabjerg, F., Hansen, S., 2005. Design and control of an LCL-filter-based three-phase active rectifier. IEEE Trans. Ind. Appl. 41 (5), 1281–1291.

Mazloomi, S.K., Sulaiman, Nasri, 2012. Influencing factors of water electrolysis electrical efficiency. Renew. Sustain. Energy Rev. Volume 16 (Issue 6), 4257–4263.

F. Meng, Z. Man and L. Gao, A 12-pulse Rectifier Based on Power Electronic Phase-shifting Transformer, 2018a IEEE International Power Electronics and Application Conference and Exposition (PEAC), Shenzhen, China, 2018, pp. 1-4, doi: ⟨10.1109/PEAC.2018.8590501⟩.

Meng, F., Xu, X., Gao, L., Man, Z., Cai, X., 2019. Dual passive harmonic reduction at DC link of the double-star uncontrolled rectifier (April). IEEE Trans. Ind. Electron. vol. 66 (4), 3303–3309. https://doi.org/10.1109/TIE.2018.2844840.

Moradi, Ramin, Groth, Katrina M., 2019. Hydrogen storage and delivery: review of the state of the art technologies and risk and reliability analysis. Int. J. Hydrog. Energy Volume 44 (Issue 23), 12254–12269.

Rivera, J., Rodriguez, J., Abu-Rub, H., Young, H.A., 2017. A comprehensive review of recent advances in matrix converter technology. IEEE Trans. Ind. Electron. 64 (7), 5396–5409.

Rodriguez, Jose, Cortes, Patricio, 2012. Predictive Control of Power Converters and Electrical Drives. Wiley.

Singh, B., Bhuvaneswari, G., Kalpana, R., 2010. Autoconnected transformerbased 18-pulse ac-dc converter for power quality improvement in switched mode power supplies (July). IET Power Electron vol. 3, 525–541 (July).

Staffell, I., Green, R., 2019. The cost of domestic fuel cell micro-CHP systems. Int. J. Hydrog. Energy 44 (1), 480–494.

Uzunoglu, M., Onar, O.C., Alam, M.S., 2009b. Modeling, control and simulation of a PV/FC/UC based hybrid power generation system for stand-alone applications. Renew. Energy Volume 34 (Issue 3), 509–520.

Uzunoglu, M., Onar, O.C., Alam, M.S., 2009a. Modeling, control and simulation of a PV/FC/UC based hybrid power generation system for stand-alone applications. Renew. Energy Vol 34 (Issue 3), 509–520.

Vazquez, S., Rodriguez, J., Rivera, M., Franquelo, L.G., Norambuena, M., 2019. Model predictive control for matrix converters: a review. IEEE Trans. Ind. Electron. 66 (1), 15–29.

Zhaksylyk, A., Rasool, H., Abramushkina, E., Chakraborty, S., Geury, T., El Baghdadi, M., Hegazy, O., 2023. Review of active front-end rectifiers in EV DC charging applications. Batteries 9 (3), 150.